Available online at www.sciencedirect.com
SCIENCE DIRECT®
Journal of Computational Physics 191 (2003) 18–39
JOURNAL OF COMPUTATIONAL PHYSICS
www.elsevier.com/locate/jcp

Finite difference heterogeneous multi-scale method for homogenization problems

Assyr Abdulle [a,*], Weinan E [b]

[a] Computational Laboratory, CoLab, ETH Zürich, CH-8092 Zurich, Switzerland
[b] Department of Mathematics and PACM, Princeton University, NJ 08544-1000, USA

Received 26 November 2002; accepted 6 May 2003

Abstract

In this paper, we propose a numerical method, the finite difference heterogeneous multi-scale method (FD-HMM), for solving multi-scale parabolic problems. Based on the framework introduced in [Commun. Math. Sci. 1 (1) 87], the numerical method relies on the use of two different schemes for the original equation, at different grid level which allows to give numerical results at a much lower cost than solving the original equations. We describe the strategy for constructing such a method, discuss generalization for cases with time dependency, random correlated coefficients, non-conservative form and implementation issues. Finally, the new method is illustrated with several test examples.

Keywords: Multi-scale problem; Homogenization; Finite difference; Heterogeneous multi-scale method

1. Introduction

This paper is devoted to the numerical solution of partial differential equations with coefficients involving different scales. Direct numerical treatments of these problems are difficult due to the cost required for resolving the smallest scale. Discrete scheme obtained in this way are often by far too expensive to be solved directly.

Analytic treatments of these problems lead to so-called homogenized equations in which the multi-scale problem, depending on small parameters, is replaced by an equation with non-oscillatory coefficients found as a limit (usually in a weak sense) when the small parameters tend to zero. These analytical techniques have been studied for many years (see for example [5,6], and the references therein). They can be successful for several applications, but are limited by restrictive assumptions on the media.

From a numerical point of view, the homogenized equations have to be obtained first and then, one has to solve the homogenized equations. It is often preferable to handle the original equations without the intermediate step through homogenization. One reason is that the aforementioned approach eliminates the

* Corresponding author. Tel.: +1-41-1-6324-502; fax: +1-41-1-6321-703.
E-mail addresses: abdulle@inf.ethz.ch (A. Abdulle), weinan@math.princeton.edu (W. E).

0021-9991/$ - see front matter © 2003 Elsevier Science B.V. All rights reserved.
doi:10.1016/S0021-9991(03)00303-6

small scales that can be of interest. In classical homogenization, the recovery of the fine scale features is done by using correctors, but these are of the same complexity as the original problem.

Numerical computation for homogenization problems was first studied by Babuska [4] for elliptic problems and Engquist [9] for dynamic problems. Babuska proposed for a linear variational homogenization problem in one dimension to use a finite element method on a macro-scale grid but with modified basis functions that are obtained from solving the original multi-scale problem with $f = 0$ as the right-hand side. With this strategy, the basis functions capture the correct microscopic behavior. These ideas were extended recently to higher dimensions by Hou et al. [14,15]. The methods based on this approach require a cost that is comparable to that of solving the original problem on a fine grid.

Another strategy based on finite element methods is that of Schwab, Matache and Babuska [18,19], using macro- and micro-shape functions on two-scale finite element space. The cost of this method is independent of the micro-scale ε but it is up to now limited to problems with periodic micro-structure. For the analytical treatment of homogenization equations, two-scale test functions were used by Nguentseng [17], E [7] and Allaire [3].

Engquist and Runborg [10,11] proposed a method based on multi-resolution analysis with wavelet projections and approximation of the discrete operator. For a given wavelet space, the discretized operator originating from the oscillating problem is projected into a coarse subspace.

Neuss et al. [20] proposed a method based on a standard finite element setting and uses a two-grid algorithm for the multigrid iteration. That is, the multigrid iteration start with the original equations (with the small scales) but the direct resolution is done for the homogenized problem.

These aforementioned techniques seem to be limited to particular classes of problems. In this paper we propose a new method, the finite difference heterogeneous multi-scale method (FD-HMM), for the numerical solution of parabolic multi-scale equations. This method is based on the framework of the heterogeneous multi-scale method (HMM) introduced in [8], a general methodology for the efficient numerical computations of problems with multiple scales. The goal is to build a method in a way that can be applied to more general problems than classical homogenization, as for example for problem with time dependent or random stationary (correlated) coefficients as well as for non-conservative problems.

There are two main components in the finite difference heterogeneous multi-scale method:

- a macroscopic scheme evolved on a coarse grid (the grid of interest) with unknown data recovered from the solutions of the microscopic model;
- a microscopic scheme, in which the original equation is solved on a sparse (heterogeneous) spatial domain.

We describe in Section 2.2 the new finite difference HMM method, explain how to overcome several issues that arise when implementing the numerical method, and give an algorithm for implementing it. Finally, we give in Section 3 numerical examples to illustrate the performance of the proposed method.

2. Finite difference and multi-scale problems

In this section, we first recall in Section 2.1 some of the basic theory of homogenization, which is an important class of problem for our new method. We then describe in Section 2.2 the method, and give several generalizations. Finally, we establish a consistency result for the method.

2.1. Classical homogenization of parabolic problems

For now, we consider the following multi-scale parabolic equation:

$$\frac{\partial u^\varepsilon}{\partial t} = \nabla \cdot \left(A\left(\frac{x}{\varepsilon}\right) \nabla u^\varepsilon \right) \quad \text{in } (0,T) \times \Omega, \tag{1}$$

$$u^\varepsilon = 0 \quad \text{on } (0,T)\times\partial\Omega, \tag{2}$$

$$u^\varepsilon(0,x) = g^\varepsilon(x) \in L^2(\Omega), \tag{3}$$

where $u^\varepsilon = u^\varepsilon(t,x)$, $x \in \Omega \subset \mathbb{R}^d$ is a bounded domain, and $A^\varepsilon(x) = A(x/\varepsilon) = (A_{ij}(\cdot))_{i,j=1}^d$ is real with $A_{ij}(\cdot) \in L^\infty(\mathbb{R}^d)$, uniformly elliptic, bounded and periodic in each of its spatial direction, i.e.,

$$\left(A\left(\frac{x}{\varepsilon}\right)\xi,\xi\right) \geqslant \alpha|\xi|^2, \quad \left|A\left(\frac{x}{\varepsilon}\right)\xi\right| \leqslant \beta|\xi| \quad \text{with } \alpha,\beta > 0, \tag{4}$$

$$A_{ij}(y_1 + l_1,\ldots,y_d + l_d) = A_{ij}(y_1,\ldots,y_d), \tag{5}$$

where we set $y_i = x_i/\varepsilon$ and $A(x/\varepsilon) = A(y)$. The functions $A_{ij}(y)$ will be referred as y-periodic functions. To simplify the notation we suppose in the sequel that $l_i = 1$.

The variational problem associated with (1)–(3) admits a unique solution $u^\varepsilon \in L^2((0,T);H_0^1(\Omega))$ and $\partial u^\varepsilon/\partial t \in L^2((0,T);H^{-1}(\Omega))$. If u^ε and $\partial u^\varepsilon/\partial t$ are in the aforementioned spaces, then u^ε is almost everywhere equal to a continuous function from $[0,T] \to L^2(\Omega)$ so that the initial values (3) for u^ε make sense (see [16] for details).

If we apply a standard finite difference scheme to Eq. (1) the discretization should satisfy $\Delta x < \varepsilon$ if we want to resolve the ε-scale, which can be prohibitive if ε is small.

Classical homogenization theory tells us that (see [5, Chapter.1.2; 6, Chapter 11])

$$u^\varepsilon \rightharpoonup u^0 \quad \text{weakly in } L^2\big((0,T);H_0^1\big), \tag{6}$$

where u^0 is the solution of the so-called homogenized problem

$$\frac{\partial u^0}{\partial t} = \nabla\cdot\left(A^0\nabla u^0\right) \quad \text{in } (0,T)\times\Omega, \tag{7}$$

$$u^0 = 0 \quad \text{on } (0,T)\times\partial\Omega,$$

$$u^0(0,x) = g^0(x) \in L^2(\Omega),$$

where we assume that $g^\varepsilon \rightharpoonup g^0(x)$ weakly in $\in L^2(\Omega)$, and A^0 is a constant matrix given by

$$A^0_{ij} = \int_Y \left(A_{ij}(y) + \sum_{k=1}^d A_{ik}(y)\frac{\partial\chi^j}{\partial y_k}(y)\right)\mathrm{d}y, \tag{8}$$

where $Y = (0,1)^d$ (we suppose $A(y)$ is 1-periodic in $y_1,\ldots,y_d$) and $\chi^j(y)$ are given by the solution of the cell problems

$$\sum_{i=1}^d \frac{\partial}{\partial y_i}\left(\sum_{k=1}^d A_{ik}\frac{\partial\chi^j}{\partial y_k}\right) = -\sum_{i=1}^d \frac{\partial}{\partial y_i}A_{ij}, \quad j = 1,\ldots,d,$$

$$\int_Y \chi^j(y)\,\mathrm{d}y = 0. \tag{9}$$

This gives in variational form

$$\int_Y \nabla\chi^j A\nabla v \,\mathrm{d}y = -\int_Y (Ae_j)^{\mathrm{T}}\nabla v \,\mathrm{d}y \quad \forall v \in W^1_{\mathrm{per}}(Y),\ j = 1,\ldots,d, \tag{10}$$

where $(e_j)_{j=1}^d$ is the canonical basis of $\mathbb{R}^d$ and $W^1_{\mathrm{per}}(Y) = \{v \in H^1_{\mathrm{per}}(Y); \int_Y v\,\mathrm{d}x = 0\}$, where $H^1_{\mathrm{per}}(Y)$ is defined as the closure of $C^\infty_{\mathrm{per}}(Y)$ (the subset of $C^\infty(\mathbb{R}^d)$ of 1-periodic functions) To obtain Eq. (8) we make the following ansatz for u^ε:

$$u^\varepsilon(t,x) = u^0(t,x) + \varepsilon u_1\left(t,x,\frac{x}{\varepsilon}\right) + \varepsilon^2 u_2\left(t,x,\frac{x}{\varepsilon}\right) + \cdots, \tag{11}$$

where the functions $u_j(t,x,y)$ are periodic in the variable y for any t and x (see for example [5, Chapter 1]). The formal procedure is then to insert (11) in (1) and to compare the power of ε. We find that $u^0(t,x)$ satisfies Eq. (7) and u_1 is given by

$$u_1(t,x,y) = \sum_{j=1}^d \chi^j(y)\frac{\partial}{\partial x_j}u^0(t,x), \tag{12}$$

where $\chi(y)$ is given by (9). For the flux defined by $p^\varepsilon(t,x) = A(x/\varepsilon)\nabla u^\varepsilon$, typical convergence result is (see [5])

$$p^\varepsilon(t,x) \to A^0\nabla u^0 \quad \text{weakly in } (L^2((0,T);\Omega))^d. \tag{13}$$

Remark 1. The classical homogenization theory still applies for non-uniformly oscillating coefficients $A_{ij}(x,x/\varepsilon)$, but then the cell problem depends on the location x, and A^0 becomes space dependent $A^0(x)$.

2.2. Finite difference HMM

To handle multi-scale problems with finite difference methods, we propose a "heterogeneous" discretization which cares about the fine scale *only on small representative region of size* ε of the spatial domain. In the following we describe in detail the algorithm sketched below, extend it to more general situation such as *non-conservative problems*, *random correlated coefficients* and *time dependent coefficients*. Finally, we give consistency results for the proposed method.

Let us first give a short overview of the strategy before giving a more detailed description. We consider the domain $\Omega = [0,1]\times[0,1]$ (for simplicity) of $\mathbb{R}^2$ and discretize it with a coarse equidistant mesh (x_{1i},x_{2j}), $i,j = 1,\ldots,N$, for which $\Delta x = x_{1i+1} - x_{1i} = x_{2j+1} - x_{2j}$ is much larger than ε.

The idea is to evolve a macroscopic model for the flux form of the parabolic equations (1)–(3)

$$\frac{\partial U}{\partial t} = \nabla\cdot P, \tag{14}$$

on a *coarse grid* with *large time step*, where $P(t,x_{1i},x_{2j}) = (P_1,P_2)$ is estimated by solving the original equation around (x_{1i},x_{2j}) in small representative regions. Notice that a macroscopic model is known to exist from the homogenization theory. The goal is to estimate it by considering only the micro-scale equations (1)–(3).

Suppose that at time t^k we have a numerical solution of Eq. (14) on the coarse grid $(x_{1i},x_{2j}) = x_{ij}$, denoted by U^k_{ij}. To find the coarse solution U^{k+1}_{ij} at time t^{k+1} we proceed in three steps:

(1) For each x_{ij}, solve Eqs. (1)–(3) on four ε-cells $I^\varepsilon_{i\pm1/2,j}, I^\varepsilon_{i,j\pm1/2}$ defined in (15) (see also Fig. 1), with corresponding solution u obtained by a finite difference method on fine spacial grid (which resolves the ε scale) for a small time step δ. The boundary conditions are such that $u(t,x) - U^k(x)$ is ε-periodic, and the initial conditions are given by $U^k(x)$, a linear reconstruction of the coarse solution U^k (on each ε-cell).

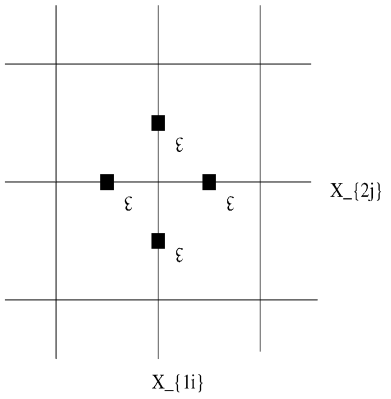

Fig. 1. ε-Cell (black boxes) at the coarse point (x_{1i}, x_{2j}).

(2) Compute

$$\nabla P_{ij} = \frac{P^k_{i+1/2,j} - P^k_{i-1/2,j} + P^k_{i,j+1/2} - P^k_{i,j-1/2}}{\Delta x} = F_{ij}(U^k),$$

where $P^k_{i+1/2,j}$ and $P^k_{i-1/2,j}$ are averages of the micro-scale flux computed with the numerical solution u given by step 1 over $I^\varepsilon_{i+1/2,j}$ and $I^\varepsilon_{i-1/2,j}$, respectively. Similarly, $P^k_{i,j+1/2}$ and $P^k_{i,j-1/2}$ are the average of the micro-scale flux computed with the numerical solution u over $I^\varepsilon_{i,j+1/2}$ and $I^\varepsilon_{i,j-1/2}$, respectively.

(3) Evolve the equation $\partial U^k/\partial t = F(U^k)$ on the coarse mesh (x_{1i}, x_{2j}) with a large time step Δt.

Standard finite difference methods would consists in discretizing the whole domain with the microscopic model and evolve the equations on it. Thus it would produce a large number of equations (if ε is small compared to Ω) difficult to solve numerically. For the proposed finite difference heterogeneous multi-scale method (FD-HMM), based on the aforementioned coupling, the main numerical work will consist in solving the microscopic model. But this is only done on small sub-domain of the original domain. Since the microscopic cell problems are independent, they can be solved in parallel, which is another advantage of that method. Notice finally that for the FD-HMM the number of equations for solving the cell problems does not depend on ε, since the ε-domain decreases if ε decreases.

We describe now this algorithm in more detail. To simplify the notation, we will usually skip the upper index corresponding to the time when it is not relevant.

Step (1) Cell problem

Let us define $d_- = (\Delta x - \varepsilon)/2, d_+ = (\Delta x + \varepsilon)/2$ and four ε-cells around each point (x_{1i}, x_{2j}):

$$\begin{aligned} I^\varepsilon_{i\pm1/2,j} &= [x_{1i} \pm d_-, x_{1i} \pm d_+] \times [x_{2j} - \varepsilon/2, x_{2j} + \varepsilon/2], \\ I^\varepsilon_{i,j\pm1/2} &= [x_{1i} - \varepsilon/2, x_{1i} + \varepsilon/2] \times [x_{2j} \pm d_-, x_{2j} \pm d_+]. \end{aligned} \tag{15}$$

We will solve the original equation on a small grid which resolve the ε scale, i.e., we resolve the ε-scale on a ε-domain. The small grid is defined by

$$(k, l) = (\xi_k, \xi_l), \quad k, l = 0, \ldots, s, \quad \text{where } \xi_m = \frac{\Delta x - \varepsilon}{2} + m\Delta\xi, \tag{16}$$

and where $\Delta\xi = \varepsilon/s$, and s is an integer chosen so that $\Delta\xi$ resolves the ε-scale.

In the sequel we denote $I^\varepsilon = I^\varepsilon_{i\pm1/2,j\pm1/2}$ a cell given by (15) and we will skip the dependency on the index $i\pm1/2,j\pm1/2$ if no confusion can occur. On each such cell we discretize (1)–(3) by the method of line and obtain the semi-discrete equation

$$\frac{\mathrm{d}}{\mathrm{d}t}u_{k,l} = \frac{1}{(\Delta\xi)^2}F_{kl}(t) \quad k,l,=1,\ldots,s, \tag{17}$$

where F_{kl} is a finite difference discretization of $\nabla\cdot(A^\varepsilon\nabla u(x_{1k},x_{1l}))$ (for example the 5-point stencil provided A^ε is diagonal, the 9-point stencil otherwise).

To start the evolution with the cell problems, we need initial values and boundary conditions which are not known for the cell problems.

(i) *Reconstruction for initial values.* We define initial values for the cell problems by a reconstruction from the values on the coarse grid, U_{ij} whose values are given from the previous step or from the initial values. The simplest reconstruction is a linear one on each cell. For example for the cell $I^\varepsilon_{i-1/2,j}$,

$$u_{kl} = U_{i-1,j} + \xi_l\frac{U_{i,j}-U_{i-1,j}}{\Delta x}, \quad l=0,\ldots,s, \tag{18}$$

where $k=0,\ldots,s$, and ξ_l is defined in (16). We will also consider $U(\xi_m,\xi_n)$ for the same reconstruction, with (ξ_m,ξ_n) defined by (16) (but on $[x_{i-1},x_i]$, where m,n can be $>s$ and also <0).

(ii) *Boundary conditions.* Next, we need boundary conditions for the cell problems. The natural boundary conditions to recover the macroscopic input data from the microscopic computation are analogous to the cell problem of the homogenization problem (see Section 2.1). This will be made clear in Section 2.3. We will use the following boundary conditions for the micro-scale solver:

$$\begin{aligned} &u_{k,-1} = u_{k,s-1} + U(\xi_k,\xi_{-1}) - U(\xi_k,\xi_{s-1}), \quad k=1,\ldots,s,\\ &u_{s+1,l} = u_{1,l} + U(\xi_{s+1},\xi_l) - U(\xi_1,\xi_l), \quad l=1,\ldots,s, \end{aligned} \tag{19}$$

with similar formulas for u_{-1l} and $u_{k,s+1}l=0,\ldots,s$ and where $U(\xi_k,\xi_l)$ denotes the linear reconstruction (18) for the the values U_{ij} on the coarse grid.

Another possibility would be to consider a discrete version of $\int_{I^\varepsilon}\nabla u\,\mathrm{d}\xi = \int_{I^\varepsilon}\nabla U\,\mathrm{d}\xi$, which is a weaker form than (19).

(ii) *Exact cell problem.* In the sequel we will also also denote by (see also (43))

$$\hat{\boldsymbol{u}}^\varepsilon(t+\delta,\xi_k,\xi_l) \tag{20}$$

the solution of Eqs. (1)–(3) at time $t+\delta$ over the cell I^ε with linear initial conditions given by the reconstruction (18) and boundary conditions such that $\hat{\boldsymbol{u}}^\varepsilon - U$ is ε-periodic (similar to 19). By standard error estimates for semi-discrete approximations we have

$$|\hat{\boldsymbol{u}}^\varepsilon(t,\xi_k,\xi_l) - u_{kl}(t)| \leqslant C(\Delta\xi)^2. \tag{21}$$

Step (2) Flux computation

For the flux computation, a point-wise flux approximation $p^\varepsilon(t,x_{1i},x_{2j}) \simeq A^\varepsilon(x_{1i},x_{2j})\,\nabla_\xi u_{ij}$ may not work for dimension higher than one (∇_ξ denotes the finite difference approximation of the gradient). An example is given in [8, Section 6.3] which shows that the flux defined in this way may not converge to the flux of the homogenized equation for $\varepsilon\to0$. The new idea here, suggested by Lemma 3 given in Section 2.3, is to compute an average flux over a ε-cell. For each cell $I^\varepsilon = I^\varepsilon_{i\pm1/2,j\pm1/2}$ we will compute an approximation of

$$\hat{P} = \frac{1}{|I^\varepsilon|}\int_{I^\varepsilon} A(\xi/\varepsilon)\nabla\hat{\boldsymbol{u}}^\varepsilon(t+\delta,\xi)\,\mathrm{d}\xi, \tag{22}$$

where $\hat{u}^\varepsilon$ is the solution defined in (20). Thus, having computed an approximation $u_{k,l}$ of $\hat{u}^\varepsilon(t+\delta,\xi_{1k},\xi_{2l})$ in each cell $I^\varepsilon_{i\pm1/2,j\pm1/2}$, $i,j=1,\ldots,N$, by step 1, we compute a discrete version of (22) written for the cell $I^\varepsilon_{i-1/2,j}$

$$P_{i-1/2,j}=\frac{(\Delta\xi)^2}{\varepsilon^2}\sum_{k,l=1}^{s}\left(A_{11}(\xi_{k+1/2},\xi_l)\frac{u_{k+1,l}-u_{k,l}}{\Delta\xi}+A_{12}(\xi_k,\xi_{l+1/2})\frac{u_{k,l+1}-u_{k,l}}{\Delta\xi}\right), \tag{23}$$

and similarly for the other quantities $P=P_{i\pm1/2,j\pm1/2}$ corresponding to the cells $I^\varepsilon_{i\pm1/2,j\pm1/2}$.

(i) *Flux equilibrium.* To compute the average (23), we have to evolve the original equation (14) on the ε-domain for a micro-time step δ. By Lemma 3 we know that

$$\hat{P}=\frac{1}{|I^\varepsilon|}\int_{I^\varepsilon}A(\xi/\varepsilon)\nabla\hat{u}^\varepsilon(t+\delta,\xi)\,\mathrm{d}\xi\to A^0\nabla u^0(t+\delta,\bar{\xi}),\quad \varepsilon\to0, \tag{24}$$

where $\bar{\xi}$ is the center of the cell I^ε, A^0 is the homogenized matrix given by (8) and u^0 is the solution of (7). The solution of the homogenized equation (7) has a steady-state flux $A^0\nabla u^0(t,x)=C(x)$, for linear initial values and the periodic boundary conditions (19). Thus by Eq. (24), $\hat{P}$ is nearly constant for small ε. But the reconstructed initial values (and the boundary conditions) can introduce transient before the computed flux P approaches a quasi-stationary state (see the numerical experiments in Section 3). The micro-time δ should be chosen so that the micro-solution reaches a quasi-equilibrium. It is discussed in [8] that (for one-dimensional problems) the "relaxation time" is of order $\mathrm{O}(\varepsilon^2)$.

(ii) *Micro-time evolution.* To reach this quasi-equilibrium state, we evolve the ODE (17) with a Runge–Kutta method over small time steps δ_t, from Δt to $\Delta t+\delta$, where $\delta=\alpha\delta_t$. The value $u_{kl}^{\Delta t+\delta}\simeq u^\epsilon(\Delta t+\delta,\ldots)$ will be used to approximate the flux on I^ε at time Δt. That is, δ does not contribute to the time evolution (we should have $\delta<\Delta t$).

The estimation of δ can be implemented in an automatic way. At the first evaluation of the microscopic equations we estimate h by finding the first α_0 such that

$$|P(t+(\alpha_0+1)\delta_t)-P(t+\alpha_0\delta_t)|\leqslant\mathrm{tol} \tag{25}$$

for a given value of tol, and we choose $\delta=\alpha_0\delta_t$.

Then the numerical solution of (17) denoted by $u_{kl}^{t+\delta}$ will introduce a time error, which for the the simplest Euler method is of order $\mathrm{O}(\delta_t)$ (after α_0 steps). And the the estimate (21) becomes for the fully discrete scheme

$$|\hat{u}(t+\delta,\xi_k,\xi_l)-u_{kl}^{t+\delta}|\leqslant C(\delta_t+(\Delta\xi)^2). \tag{26}$$

Step (3) Time evolution on the coarse grid

The time evolution on the macroscopic grid is now done via the approximation

$$\frac{\mathrm{d}U_{ij}}{\mathrm{d}t}(t)=\frac{P_{i+1/2,j}-P_{i-1/2,j}+P_{i,j+1/2}-P_{i,j-1/2}}{\Delta x}=F_{ij}(t,U),\quad i,j=1,\ldots,N, \tag{27}$$

where $P_{i\pm1/2,j\pm1/2}$ is given by (23). Notice that Eq. (27) can be written in the form of an autonomous ordinary differential equation

$$\frac{\mathrm{d}U}{\mathrm{d}t}(t)=\nabla P=F(U(t)),\quad F:\mathbb{R}^{N^2}\to\mathbb{R}^{N^2}, \tag{28}$$

where F is defined by (27). Notice that F is continuous (differentiable) if the coefficients $A^\varepsilon_{ij}(x)$ of (1) are smooth enough. Indeed, F is a composition of continuous (differentiable) maps

$$F : \mathbb{R}^{N^2} \xrightarrow[\text{reconstruction}]{} \mathbb{R}^{s^2 \cdot 2N(N+1)} \xrightarrow[\text{ODE solution}]{} \mathbb{R}^{s^2 \cdot 2N(N+1)} \xrightarrow[\text{flux estimation}]{} \mathbb{R}^{N^2}.$$

Time evolution with Runge–Kutta methods. The simplest fully discrete scheme which evolves the coarse solution from time step t_k to $t_{k+1} = t_k + \Delta t$ is given by the Euler method

$$U_{ij}^{k+1} = U_{ij}^k + \Delta t \cdot F_{ij}^k, \tag{29}$$

where $F_{ij}^k = F_{ij}(U^k)$. To implement a higher order m-stage explicit Runge–Kutta method, we have to compute successively the functions

$$K_i = F\left(U^k + \sum_{j=1}^{i-1} a_{ij} K_j\right), \quad i = 1, \ldots, m, \tag{30}$$

at intermediate stages K_i, where $K_1 = F(U^k)$ (see [12, Chapter 2] for details). For each evaluation of the intermediate stages K_i, we need to evaluate the function F with the algorithm explained above.

2.2.1. Generalization

In the following, we show that the same ideas as explained above apply, with some modifications, to more general situations as *non-conservative problems*, *random stationary correlated coefficients*. They also apply readily for *time dependent coefficients*.

2.2.2. Non-conservative problems

Consider for example

$$\frac{\partial u^\varepsilon}{\partial t} = \sum_{i,j} a_{ij}\left(x, \frac{x}{\varepsilon}\right) \frac{\partial^2 u^\varepsilon}{\partial x_1 \, \partial x_2}(x,t), \tag{31}$$

where $x = (x_1, x_2)$. We can think of the macro-scale model, the homogenized equation, abstractly as

$$\frac{\partial U}{\partial t} = F(U), \tag{32}$$

where F is some unknown linear operator. For the macro-scale scheme, we choose an ODE solver, for example the Euler method

$$U_{ij}^{k+1} = U_{ij}^k + \Delta t F_{ij}(U^k), \tag{33}$$

where $F_{ij}(U^k)$ is an approximation to $F(U^k)$ at the (i,j)th grid point x_j.

Our next task is to estimate $F(U^k)$ in order to give an expression for $F_{ij}(U^k)$. This can be done as follows.

Step (1) Cell problem. Reconstruction: from $\{U_{ij}^k\}$, the known numerical solution at time step t_k, reconstruct a piecewise quadratic polynomial $U^k(x)$, such that (written here for the x_1 direction)

$$U^k(x_{ij}) = U_{ij}^k, \qquad \frac{\partial U^k}{\partial x}(x_{ij}) = \frac{U_{i+1,j}^k - U_{i-1,j}^k}{2\Delta x}, \tag{34}$$

$$\frac{\partial^2 U^k}{\partial x^2}(x_{ij}) = \frac{U_{i+1,j}^k + -2U_{ij}^k + U_{i-1,j}^k}{\Delta x^2}. \tag{35}$$

Solve (31) on the domain $I^\varepsilon = x_{ij} + \varepsilon I$, where $I = [-1/2, 1/2] \times [-1/2, 1/2]$, with initial condition $u(x, t^k) = U^k(x)$, and boundary condition so that $u(x,t) - U^k(x)$ is periodic with period εI.

Step (2) Force computation. Compute a discrete version of

$$F_{ij}(U^k) = \frac{1}{|I^\varepsilon|}\int_{I^\varepsilon} \sum_{k,l} a\Big(x, \frac{x}{\varepsilon}\Big) \frac{\partial^2 u^\varepsilon}{\partial x_1\, \partial x_2}(x, t^k + \delta)\, \mathrm{d}x, \tag{36}$$

for suitably chosen δ, where u is the solution obtained at Step 2 and where $|I^\varepsilon|$ denotes the measure of I^ε. α should be chosen such that $F_{ij}(U^k)$ reaches a quasi-stationary value (see subsection *Micro-time evolution*).

Step (3) Time evolution on the coarse grid. Evolve (33) on the coarse mesh with a large time step.

2.2.3. Random coefficient

The FD-HMM method can be applied for some problems with random coefficients. For example in the case where the random coefficients $a^\varepsilon(x)$ are known to have a correlation length ε. Step 1 of the method applies without modification, either as described above (non-conservative equation) or as described previously.

For Step 2, the ε-cell, whose size was given in the periodic case by the length of the period is now given by the correlation length. Unlike the periodic case, one should consider the microscopic solver on domains larger than one cell in order to have enough information from the microscopic equations (see numerical example in Section 3).

Finally Step 3, the evolution of the ODE on the coarse mesh can be done similarly as explained above.

2.2.4. Time dependent coefficients

The FD-HMM applies readily for *time dependent* coefficients $A^\varepsilon(x,t)$, in conservative or non-conservative problems and also in the case of random coefficients. In these situations, at each coarse step, the algorithm for computing the flux or the forces has to be applied.

2.2.5. Estimation of the macro-scale coefficients

In some situation, for example for *time independent* coefficients, it is only necessary to apply the microscopic solver once. Indeed, knowing P_{ij} (an approximation of the flux $A^0\nabla u^0$ of the homogenized equation) and u_{ij} on a cell (after applying the microscopic solver), we can estimate the coefficients (A_{ij}) of the unknown macroscopic model

$$\frac{\mathrm{d}U}{\mathrm{d}t}(t) = \nabla P = \nabla\cdot(A\nabla U). \tag{37}$$

For example we obtain A_{11}, A_{12} by solving a linear system for two different cells around (x_{1i}, x_{2j}),

$$P_1 = A_{11}\partial_1 U + A_{12}\partial_2 U \quad \text{on } I^\varepsilon_{i+1/2,j}, \tag{38}$$

$$\tilde{P}_1 = A_{11}\partial_1 \tilde{U} + A_{12}\partial_2 \tilde{U} \quad \text{on } I^\varepsilon_{i-1/2,j}, \tag{39}$$

where $P = (P_1, P_2)$, $\tilde{P} = (\tilde{P}_1, \tilde{P}_2)$ are the computed flux with the microscopic solver on the cell $I^\varepsilon_{i+1/2,j}$ and $I^\varepsilon_{i-1/2,j}$, respectively, and U is the macroscopic available solution. Similarly we get the entries A_{21}, A_{22}.

2.2.6. Recover the small-scale information

It can sometimes be of interest to recover information about the small scale at some points outside the coarse mesh.

Let $\Delta x = x_{i,j} - x_{i-1,j}$ be the size length of the coarse grid mesh. Let u_{kl_0} be the solution of Eq. (17) on the cell $x_{i-1/2,j} + \varepsilon\cdot[-1/2, 1/2]$, where the index l_0 corresponds to the index of the middle of the cell with respect to the x_2 axis. We extend periodically the obtained micro-scale values u_{kl_0} on $[x_{1,i-1}, x_{2j}]$ as

$$\tilde{u}_{ml_0} = U(\xi_m, \xi_{l_0}) + (u_{k_m,l_0} - U(\xi_{k_m}, \xi_{l_0})),$$

where for $m \in \mathbb{Z}$, $k_m \in \{0, \ldots, s\}$ is given by $k_m \equiv m(s+1)$ and $U(\xi)$ is given by the reconstruction defined in (18).

2.2.7. Summary of the algorithm

We summarize our algorithm for the solution of a parabolic multi-scale equations on a domain Ω: define a coarse discretization $(x_{1i}, x_{2j}), i, j = 1, \ldots, N$ of the domain Ω, and $2N(N+1)$ cells I^ε (see Fig. 1) with length and width of size comparable to ε, discretized with $(\xi_{1l}, \xi_{2m}),\ l, m = 1, \ldots, s$.

(1) Solve the original equation on each cell I^ε, with initial solution given by the piecewise linear reconstruction (18) in case of conservative problem and piecewise quadratic reconstruction (34) in case of non-conservative problem, with boundary conditions (19).
(2) Compute the flux approximation (23) or the force approximation (36).
(3) Evolve the ODE of the macroscopic model (28) or (32) on the coarse mesh $(x_{1i}, x_{2j}),\ i, j = 1, \ldots, N$.

The first saving in computation time in the FD-HMM strategy is achieved by reducing the computation of the micro-scale on micro-domain (step 1). Notice that each ε-cell computation is independent, so that the computation of the ε-cell problems can be done in parallel. Since the macro computation (step 3) is very fast the parallel implementation can highly speed up the computation time.

2.3. Consistency results

The error between the results given by the FD-HMM and the homogenized equation several parts:

- the error between the estimated flux and the homogenized flux;
- the error given by the macro-scale solver.

We will, as suggested in [8], compare the solution given by the FD-HMM method (see (29))

$$U_{ij}^{k+1} = U_{ij}^k + \Delta t \cdot F_{ij}^k, \tag{40}$$

with a macroscopic scheme

$$\bar{U}_{ij}^{k+1} = \bar{U}_{ij}^k + \Delta t \cdot \bar{F}_{ij}^k, \tag{41}$$

chosen such that the micro-scale solver in the algorithm (on the ε-cell) is replaced by the solution of the homogenized equations, on the same ε-cell with the same boundary conditions (19). As in (27), we write

$$\bar{F}_{ij}^k = \frac{\bar{P}_{i+1/2,j}^k - \bar{P}_{i-1/2,j}^k + \bar{P}_{i,j+1/2}^k - \bar{P}_{i,j-1/2}^k}{\Delta x}, \tag{42}$$

where $\bar{P}_{ij}$ will be explicitly given (see 44).

The analysis given in [8] is done for the parabolic case in one dimension using a different approximation for the flux as in the FD-HMM and cannot be generalized to higher dimension. We discuss here the case of higher dimension, with the new flux approximation (22).

Let us write

$$U^k = (U_{11}, \ldots, U_{1N}, \ldots, U_{N1}, \ldots, U_{NN})^{\mathrm{T}} \in \mathbb{R}^{N^2}.$$

For the flux

$$P_{i\pm1/2,j\pm1/2}(U^k) \quad \text{and} \quad \bar{P}_{i\pm1/2,j\pm1/2}(\bar{U}^k),$$

given by (27) and (42), respectively. In the sequel we will skip the dependency toward U^k and denote the time dependency t^k as a superscript $P^k, \bar{P}^k$. We will also denote by C a generic constant whose value can

change at any occurrence but depends only on the quantities which are indicated explicitly. By (27) and (42) it is sufficient to estimate $|P^k_{i\pm1/2,j\pm1/2} - \bar{P}^k_{i\pm1/2,j\pm1/2}|$.

Let t^k be fixed and U^k be the solution given by the FD-HMM at time t^k, and $U^k(x)$ be the piecewise linear reconstruction of this solution given by (18). Recall that in (20) we have defined $\hat{\boldsymbol{u}}^\varepsilon$ the solution of

$$\begin{cases} \frac{\partial \hat{\boldsymbol{u}}^\varepsilon}{\partial t} = \nabla \cdot (A^\varepsilon \nabla u^\varepsilon), \quad (t,x) \in (t^k, t^k+\delta) \times I^\varepsilon_{i\pm1/2,j\pm1/2}, \\ \hat{\boldsymbol{u}}^\varepsilon - U^k(x), \quad \varepsilon\text{-periodic on } I^\varepsilon_{i\pm1/2,j\pm1/2}, \\ \hat{\boldsymbol{u}}(t^k,x) = U^k(x), \end{cases} \tag{43}$$

where $I^\varepsilon_{i\pm1/2,j\pm1/2}$ is a ε-cell defined in (15) and δ is the relaxation time (see (25)). To simplify we will skip the dependency on the index $_{i\pm1/2,j\pm1/2}$ when no confusion can occur.

Let $\bar{U}^k(t,x)$ be the solution of the above problem but with A^ε replaced by A^0 the homogenized matrix associated to (1)–(3). Then for these linear initial conditions, $\bar{U}^k(t,x) = U^k(x)$. Thus if we define $\bar{P}_1(x_{1i},x_{2j}), \bar{P}_2(x_{1i},x_{2j})^{\mathrm{T}} = A^0 \nabla U^k(x_{1i},x_{2j})$, the flux of Eq. (42) is given by

$$\bar{P}^k_{i\pm1/2,j} = \bar{P}_1(x_{1i} \pm \Delta x/2, x_{2j}) \quad \text{and} \quad \bar{P}^k_{i,j\pm1/2} = \bar{P}_2(x_{1i}, x_{2j} \pm \Delta x/2). \tag{44}$$

To be well defined, the scheme (42) needs to be stable. If we transform the constant matrix A^0 in diagonal form (recall that A^0 is symmetric), the scheme (42) can be written as

$$\bar{U}^{k+1} = \bar{U}^k + \frac{\Delta t}{(\Delta x)^2} S \bar{U}^k, \tag{45}$$

where S is a $N^2 \times N^2$ matrix. The above scheme is stable if for all eigenvalues λ_l of S, we have

$$\left| \Delta t \frac{\lambda_l}{(\Delta x)^2} + 1 \right| \leqslant 1.$$

Let us define the space of functions

$$W(I^\varepsilon) = \left\{ v \in H^1_{\mathrm{per}}(I^\varepsilon); \int_{I^\varepsilon} v \, \mathrm{d}x = 0 \right\},$$

where $H^1_{\mathrm{per}}(I^\varepsilon)$ is defined as the closure of $C^\infty_{\mathrm{per}}(I^\varepsilon)$ (the subset of $C^\infty(\mathbb{R}^2)$ of ε-periodic functions) for the H^1 norm. By the change of variable $y = x/\varepsilon$ we have corresponding spaces over the domain $Y = (0,1)^2$ for 1-periodic functions.

Multiplying (43) by test functions in $W(I^\varepsilon)$ and integrating by part we obtain that $\hat{\boldsymbol{u}}^\varepsilon$ satisfies at $t+\delta$ $\forall z \in W(I^\varepsilon)$

$$B(\hat{\boldsymbol{u}}^\varepsilon, z) = \int_{I^\varepsilon} A(x/\varepsilon) \nabla \hat{\boldsymbol{u}}^\varepsilon(t^k+\delta,x) \nabla z(x) \, \mathrm{d}x = -\int_{I^\varepsilon} \frac{\partial \hat{\boldsymbol{u}}^\varepsilon(t^k+\delta,x)}{\partial t} z(x) \, \mathrm{d}x. \tag{46}$$

In the sequel we set $h(x) = \partial \hat{\boldsymbol{u}}^\varepsilon(t^k+\delta,x)/\partial t$, and we skip the dependence on t. We will call δ the relaxation time. It is the time (if it exists) for which u^ε reaches a quasi-stationary value. Notice that $\hat{\boldsymbol{u}}^\varepsilon - U^k$ is periodic on I^ε and we set

$$\hat{\boldsymbol{u}}^\varepsilon = U^k + \hat{\psi} \quad \text{and} \quad \psi = \left(\hat{\psi} - \int_{I^\varepsilon} \hat{\psi} \, \mathrm{d}x \right) \in W(I^\varepsilon). \tag{47}$$

Assumption. In the sequel we assume that

$$\text{(A)} \qquad h(\cdot) := \frac{\partial \hat{u}^\varepsilon}{\partial t}(t+\delta,\cdot) \in L^\infty(I^\varepsilon) \quad \text{and} \quad \|h\|_{L^\infty(I^\varepsilon)} = -\eta_\delta \leqslant \varepsilon,$$

where η_δ depends on the relaxation time δ. If u^ε reaches a quasi-stationary value for $t \to t^k + \delta$ then $\eta_\delta \to 0$. Numerical experiments (see Fig. 2 in Section 3) indicates that the relaxation time is of order ε^2. This was discussed in [8] for the one dimension case.

We next define another function $\tilde{u}^\varepsilon$ which will be used in the following analysis. Let $\tilde{u}^\varepsilon \in U^k + W(I^\varepsilon)$ be the solution of

$$B(\tilde{u}^\varepsilon, z) = \int_{I^\varepsilon} A(x/\varepsilon)\nabla\tilde{u}^\varepsilon \nabla z \,\mathrm{d}x = 0 \quad \forall z \in W(I^\varepsilon). \tag{48}$$

This can be reformulated as follows: find $\chi^j \in W(I^\varepsilon),\ j = 1,2$ such that (see (10))

$$\int_{I^\varepsilon} A(x/\varepsilon)\nabla\left(\chi^j \frac{\partial U^k}{\partial x_j}\right)\nabla z \,\mathrm{d}x = -\int_{I^\varepsilon} A(x/\varepsilon)\left(e_j \frac{\partial U^k}{\partial x_j}\right)\nabla z \,\mathrm{d}x \quad \forall z \in W(I^\varepsilon). \tag{49}$$

Using (49) a direct calculation shows that $\tilde{u}^\varepsilon = U^k(x) + \varepsilon\sum_{j=1}^2 \chi^j(x/\varepsilon)(\partial U^k(x)/\partial x_j)$. Then, integrating $A(x/\varepsilon)\nabla\tilde{u}^\varepsilon$ and using (8) we find

$$\frac{1}{|I^\varepsilon|}\int_{I^\varepsilon} A^\varepsilon \nabla\tilde{u}^\varepsilon \,\mathrm{d}x = A^0 \nabla U^k, \tag{50}$$

where A^0 is the constant matrix given by (8).

To estimate $|P^k_{i\pm1/2,j\pm1/2} - \bar{P}^k_{i\pm1/2,j\pm1/2}|$ we start with the following lemma.

Lemma 2. *Assume assumption (A) holds. Then we have*

$$\|\hat{u}^\varepsilon - \tilde{u}^\varepsilon\|_{H^1(I^\varepsilon)} \leqslant C\sqrt{|I^\varepsilon|}\varepsilon,$$

where $\hat{u}^\varepsilon$, $\tilde{u}^\varepsilon$ are given by (46) *and* (48), *respectively, and $|I^\varepsilon|$ denotes the measure of I^ε.*

Proof. Let $x_i \in I^\varepsilon$. We have

$$\begin{aligned}\alpha\|\hat{u}^\varepsilon - \tilde{u}^\varepsilon\|^2_{H^1(I^\varepsilon)} &\leqslant B(\hat{u}^\varepsilon - \tilde{u}^\varepsilon, \hat{u}^\varepsilon - \tilde{u}^\varepsilon) = B(\hat{u}^\varepsilon, \hat{u}^\varepsilon - \tilde{u}^\varepsilon) - B(\tilde{u}^\varepsilon, \hat{u}^\varepsilon - \tilde{u}^\varepsilon) = B(\hat{u}^\varepsilon, \hat{\psi} - \chi)\\ &= \int_{I^\varepsilon} h(x)(\hat{\psi} - \chi)dx \leqslant \left(\int_{I^\varepsilon} |h(x)|^2 \,\mathrm{d}x\right)^{1/2}\left(\int_{I^\varepsilon} |(\hat{\psi} - \chi)|^2 dx\right)^{1/2} \leqslant \sqrt{|I^\varepsilon|}\ \varepsilon\|\hat{u}^\varepsilon - \tilde{u}^\varepsilon\|_{H^1(I^\varepsilon)},\end{aligned}$$

where $\|\ \|_{H^1(I^\varepsilon)}$ denotes the usual norm on the Sobolev space $H^1(I^\varepsilon)$ and where we have used assumption (A). We have also used that $\nabla(\hat{u}^\varepsilon - \tilde{u}^\varepsilon) = \nabla(\psi - \chi)$ and thus $B(\tilde{u}^\varepsilon, \hat{u}^\varepsilon - \tilde{u}^\varepsilon) = 0$ from (48). Then dividing by $\|\hat{u}^\varepsilon - \tilde{u}^\varepsilon\|_{H^1(I^\varepsilon)}$ gives the result. □

In the next lemma we estimate the difference between the flux given by the HMM scheme with the flux of the macro scheme given by (42).

Lemma 3. *Assume assumption (A) holds. Then we have*

$$\left|\left(\frac{1}{I^\varepsilon}\int_{I^\varepsilon} A^\varepsilon \nabla\hat{u}^\varepsilon \,\mathrm{d}x - A^0\nabla U^k\right)_i\right| \leqslant C\varepsilon, \tag{51}$$

where $i = 1,2$ denotes the coordinate of the flux.

Proof. We define $w = \hat{\boldsymbol{u}}^\varepsilon - \tilde{\boldsymbol{u}}^\varepsilon$. Using (50) and Lemma 2 we obtain

$$\begin{aligned}
\left|\left(\frac{1}{|I^\varepsilon|}\int_{I^\varepsilon} A^\varepsilon \nabla \hat{\boldsymbol{u}}^\varepsilon \,\mathrm{d}x - A^0 \nabla U^k\right)_i\right| &= \left|\left(\frac{1}{|I^\varepsilon|}\int_{I^\varepsilon} A\Big(\frac{x}{\varepsilon}\Big)\nabla w \,\mathrm{d}x\right)_i\right| \\
&= \left|\frac{1}{|I^\varepsilon|}\left(\int_{I^\varepsilon}\sum_j A_{ij}\Big(\frac{x}{\varepsilon}\Big)\frac{\partial w}{\partial x_j}\,\mathrm{d}x\right)_i\right| \\
&\leqslant \frac{1}{|I^\varepsilon|}\left(\int_{I^\varepsilon}\sum_j \left|A_{ij}\Big(\frac{x}{\varepsilon}\Big)\right|^2 \mathrm{d}x\right)^{1/2}\left(\int_{I^\varepsilon}\sum_j\left|\frac{\partial w}{\partial x_j}\right|^2 \mathrm{d}x\right)^{1/2} \\
&\leqslant \frac{1}{|I^\varepsilon|}\left(\int_{I^\varepsilon}\max_{x,i,j}\left|A_{ij}\Big(\frac{x}{\varepsilon}\Big)\right|^2 \mathrm{d}x\right)^{1/2}\|\nabla w\|_{L^2(I^\varepsilon)} \\
&\leqslant C\frac{1}{\sqrt{|I^\varepsilon|}}\|\nabla(\hat{\boldsymbol{u}}^\varepsilon - \tilde{\boldsymbol{u}}^\varepsilon)\|_{L^2(I^\varepsilon)} \leqslant C\frac{1}{\sqrt{|I^\varepsilon|}}\|\hat{\boldsymbol{u}}^\varepsilon - \tilde{\boldsymbol{u}}^\varepsilon\|_{H^1(I^\varepsilon)} \leqslant C\varepsilon,
\end{aligned} \tag{52}$$

where we have used Lemma 2 in the last inequality. □

We will now estimate the difference between U^{k+1} and $\bar{U}^{k+1}$. Let us define

$$\begin{aligned}
P_1^k(x_{1i\pm 1/2}, x_{2j}) &= \left(\frac{1}{|I^\varepsilon|}\int_{I^\varepsilon_{i\pm 1/2,j}} A^\varepsilon \nabla \hat{\boldsymbol{u}}^\varepsilon dx\right)_1, \\
P_2^k(x_{1i}, x_{2j\pm 1/2}) &= \left(\frac{1}{|I^\varepsilon|}\int_{I^\varepsilon_{i,j\pm 1/2}} A^\varepsilon \nabla \hat{\boldsymbol{u}}^\varepsilon dx\right)_2,
\end{aligned}$$

and

$$P^k_{i\pm 1/2,j} = P_1^k(x_{1i} \pm \Delta x/2, x_{2j}) \quad \text{and} \quad P^k_{i,j\pm 1/2} = P_2^k(x_{1i}, x_{2j} \pm \Delta x/2). \tag{53}$$

The flux of the FD-HMM method is the discrete version of (53) (see 22). We can use standard estimates for the error between the true solution and the numerical solution of problem (43), since for the flux approximation on the ε-cell we resolve the small-scale (see also the estimates (21) and (26)). We suppose in the sequel that the macro solution U^k_{ij} is computed with fluxes $P^k_{i\pm 1/2,j\pm 1/2}$ given by (53).

Theorem 4. *Assume that assumption (A) hold, that $U^0_{ij} = \bar{U}^0_{ij}$ and that the scheme (41) is stable. Assume also that U^{k+1}_{ij} is obtained with fluxes $P^k_{i\pm 1/2,j\pm 1/2}$ given by (53) for $k = 1,\ldots,n$. Then we have*

$$|U^n_{ij} - \bar{U}^n_{ij}| \leqslant \frac{C}{\Delta x} T\varepsilon, \tag{54}$$

where $T = n\Delta t$.

Proof. To estimate the difference between (40) and (41) we have to estimate the difference $|P^k_{i\pm 1/2,j\pm 1/2} - \bar{P}^k_{i\pm 1/2,j\pm 1/2}|$. Using Lemmas 2 and 3 we have

$$|P^k_{i\pm 1/2,j\pm 1/2} - \bar{P}^k_{i\pm 1/2,j\pm 1/2}| \leqslant C^k\varepsilon,$$

where C^k is given in Lemma 2. Thus $|F_{ij}^k - \bar{F}_{ij}^k| \leqslant C^k \varepsilon/\Delta x$. If we define $C = \max_{j \leqslant n} C^j$, we obtain for the difference the schemes (40) and (41)

$$|U_{ij}^{k+1} - \bar{U}_{ij}^{k+1}| \leqslant \frac{C}{\Delta x}\varepsilon\Delta t + |U_{ij}^k - \bar{U}_{ij}^k|,$$

and by induction

$$|U_{ij}^n - \bar{U}_{ij}^n| \leqslant \frac{C}{\Delta x} T\varepsilon,$$

where $T = n\Delta t$. □

This result shows that the FD-HMM is consistent (under the hypothesis (A)) with the macro-scale scheme obtained by using the homogenized solution for the micro-solver.

In Section 3 we will give numerical results which show the dependence on ε and on the space discretization of the error between the FD-HMM and the homogenized solutions.

3. Numerical experiments

In this section, we discuss the application of the proposed algorithm at several examples.

3.1. Implementation

The algorithm of Section 2.2 has been implemented in a FORTRAN code. Since we are interested here to investigate the algorithm, we implemented a simple scheme for the macroscopic equation, that is the Euler forward method. It can be generalized to higher order methods. We also for the same reasons did our test with constant step size. For the microscopic solver, there are some situations (two dimensions, very small ε) where even for a very short time and a small domain it is advantageous to use a method with more stability (the eigenvalues of the Jacobian increase quadratically with the mesh size). If we want to keep explicit methods, then Chebyshev type methods (see [1,2] and also [13]) are indicated. They are explicit Runge–Kutta methods with extended stability regions along the negative real axis, suitable for the time integration of (space) discretized parabolic equations.

Comparison. Because it is difficult to construct interesting multi-scale problems with an exact solution, we will compare the result obtained by the FD-HMM with a computed reference solution which resolves the small scale. The Chebyshev method ROCK4 (see [1]) has been used for computing reference solutions via scale resolution. We will often refer to this solution as the "exact" solution. In one dimension (for the period case, where the oscillating coefficient is time independent), the homogenized equation is easy to compute. In this case, we will compare our obtained result with the reference and the homogenized solutions.

As a measure for the error we take the relative Euclidean norm and the maximum norm

$$\mathrm{err}_2 = \sqrt{\frac{1}{N}\sum_{i=1}^{N}\left(\frac{U_i - U(x_i)}{U(x_i)}\right)^2}, \quad \mathrm{err}_\infty = \max_{i=1,\ldots,N} |U_i - U(x_i)|, \tag{55}$$

respectively, where $U(x_i)$ denotes the reference solution (or the homogenized) solution projected on the coarse mesh.

For all computations with mesh refinement, we did a projection on the coarsest grid and compute the error on that grid (usually $N = 9$ for one dimension and $N = 81$ for two dimensions).

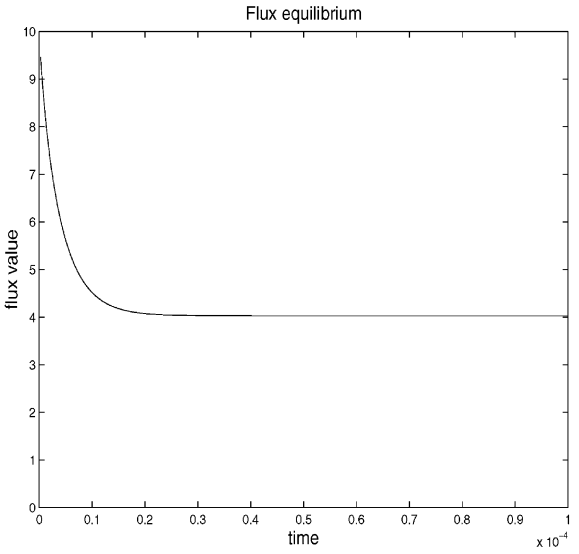

Fig. 2. The average flux $P(t) = \sum_{i=1}^{s} a^{\varepsilon}(x_i)(\mathrm{d}/\mathrm{d}x)u(t,x_i)$ for the first ε cell.

3.2. Example 1: periodic coefficient

Consider the following model problem in one dimension

$$u_t(t,x) = \frac{\mathrm{d}}{\mathrm{d}x}\left(a^{\varepsilon}(x)\frac{\mathrm{d}}{\mathrm{d}x}u^{\varepsilon}(t,x)\right), \tag{56}$$

where $a^{\varepsilon}(x) = 1.1 + \sin(2\pi x/\varepsilon)$, $\varepsilon = 10^{-2}$, with initial condition

$$u(0,x) = 10x(1-x^2), \tag{57}$$

and boundary conditions

$$u(t,0) = u(t,1) = 0 \tag{58}$$

for $0 \leqslant x \leqslant 1$ and $0 \leqslant t \leqslant 1$.

The homogenized solution is computed from Eq. (56), where the oscillating coefficient a^{ε} is replaced by its weakly convergent limit (see (8))

$$a = \left(\int_0^1 \frac{1}{1.1 + \sin 2\pi y}\,\mathrm{d}y\right)^{-1}. \tag{59}$$

For this problem, the homogenized and the reference solution, computed on a grid with $\Delta x = 1/2000$, are very close for the chosen ε. The error between both solutions is $\mathrm{err}_2 = 8.7 \times 10^{-5}$ and $\mathrm{err}_\infty = 2.4 \times 10^{-6}$ for the weighted Euclidean and maximum norm, respectively. For the computation of the flux, we proceed as explained in Section 2.2. We see in Fig. 2 that after a short transient $P(t)$, the microscopic flux is quasi-stationary. We choose the value $h = 3\mathrm{E}-5$ for the micro-time step.

The coarse solution is evolved on a spatial grid of nb interior points, thus $\Delta x = 1/(nb+1)$. For the ε-cell computation on $nb+1$ domains of length $\varepsilon = 0.01$, we solve the original equations with a mesh of size $\Delta\xi = \varepsilon/nres$. The main cost in the FD-HMM is the solution of the $(nb+1)$ cell problems and the number of

equations for it is $(nb+1)\times(nres+1)$. Notice that it is independent of ε. For example if $nb=9$ and $nres=20$, it leads to 210 equations, while for the resolution of the original equations by standard FD methods and with the same fine resolution as used in the micro-solver, it would need 1999 equations.

The time evolution of the solution (from $t=0$ to $t=1$) is done in 1000 steps, so that the coarse time step is given by $\Delta t = 1\times 10^{-3}$. We plot in Fig. 3 (left picture) the results at $t=1$ for the reference solution and for the solution of the FD-HMM. We see that the FD-HMM is able to approximate the exact solution on a coarse grid. The computational cost is much lower than a traditional method which would require the full resolution of the ε-scale. In Fig. 3 (right picture) we plot a similar computation but for a refined coarse mesh with 19 interior points. We see that the error decreases.

We now show the results of several experience with this simple equation, useful for the understanding of the algorithm and the accuracy of the FD-HMM which was discussed in Section 2.3.

First if we take smaller time step for a given mesh the method converge to the underlying ordinary differential equations (quite slowly due to the first order of the method). The error with the homogenized (or the reference) solution does not decrease (see Table 1). Notice that for a higher Runge–Kutta method, it would converge much faster to the underlying ODE.

Next we refine the coarse mesh. Until the error introduced by the spatial discretization is larger than the error introduced by the reconstruction and the flux, the error decreases. It later reaches a point where

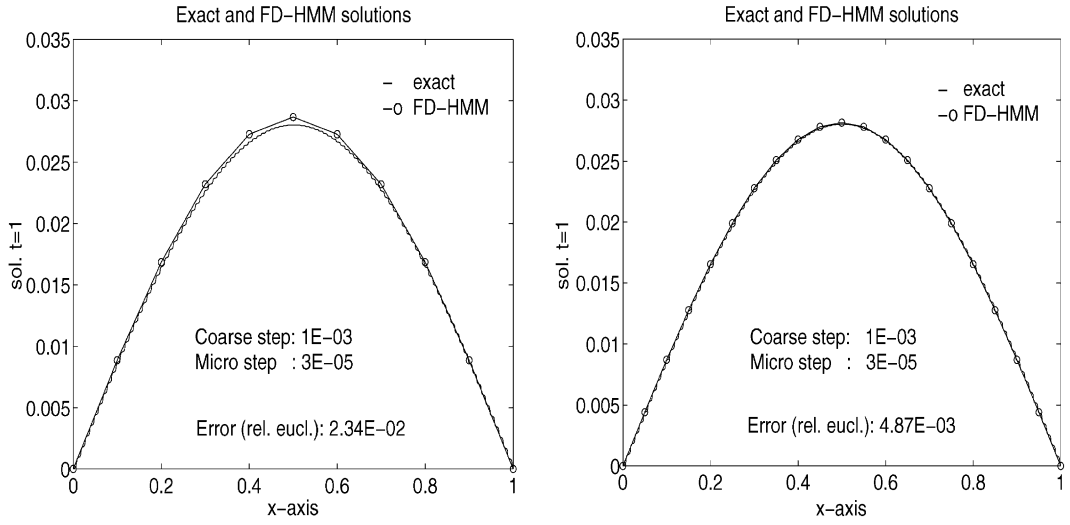

Fig. 3. Exact and FD-HMM solutions for $u_t = (\mathrm{d}/\mathrm{d}x)(a^\varepsilon(x)(\mathrm{d}/\mathrm{d}x)u^\varepsilon)$.

Table 1
Error between homogenized solution and FD-HMM for decreasing time step $\Delta t = 1/nstep$, $nb=9$ coarse points (spatial discretization), $\varepsilon = 0.01$

nstep	Error (Euclidean)	Error (maximum)
1000	2.3372×10^{-2}	6.5479×10^{-4}
5000	3.1686×10^{-2}	8.8773×10^{-4}
10,000	3.2728×10^{-2}	9.1690×10^{-4}
20,000	3.3248×10^{-2}	9.3149×10^{-4}
30,000	3.3422×10^{-2}	9.3635×10^{-4}

further refinement gives no amelioration (see Table 2). Here we took $nstep = 30{,}000$ (due to the first order of the RK-method) in order that the time error does not interfere with the other errors.

We finally decrease ε to 0.005 and we see in Table 3 that the error keeps decreasing for finer mesh size than before. As explained in Section 2.2, for time independent oscillating coefficients, the micro-solver can be applied only once.

Time dependent coefficient. We take the same example as before but with add a time dependency in the oscillating coefficients

$$a^{\varepsilon}(t,x) = (1.1 + \sin(2\pi x/\varepsilon)) \cdot (t + 0.1), \tag{60}$$

where $\varepsilon = 10^{-2}$ as before. In this case, the homogenization is not straightforward (in particular the coefficient given by (59) has to be computed at each time step). The FD-HMM applies without modification. The unique difference is that the relaxation time can depend on t and should be for efficiency computed several times during the integration process. For this example it is between 2×10^{-4} (in the beginning) and 3×10^{-5} (at the end). We show in Table 4 the obtained results. The macro time step is $\Delta t = 1 \times 10^{-3}$ for $N = 1, \ldots, 29$.

Small scale recovery. As explained in Section 2.2, to have a solution on the whole spatial domain, we do a periodic extension of the solution computed in the ε- cell. We choose the above problem with time independent coefficient. In Table 5 we give the error of such extended solutions on a fine grid with $\Delta x = 1/2000$,

Table 2
Error between homogenized solution and FD-HMM for increasing number of coarse steps (spatial discretization), $\varepsilon = 0.01$

nb Coarse	Error (Euclidean)	Error (maximum)
9	3.3422×10^{-2}	9.3635×10^{-4}
19	5.1147×10^{-3}	1.4329×10^{-4}
29	1.1901×10^{-3}	3.3342×10^{-5}
39	1.8688×10^{-3}	5.2355×10^{-5}
49	2.7043×10^{-3}	7.5763×10^{-5}

Table 3
Error between homogenized solution and FD-HMM for increasing number of coarse steps (spatial discretization), $\varepsilon = 0.005$

nb Coarse	Error (Euclidean)	Error (maximum)
9	3.6075×10^{-2}	1.0107×10^{-4}
19	7.7111×10^{-3}	2.1604×10^{-4}
29	3.7964×10^{-3}	1.0637×10^{-4}
39	7.1352×10^{-4}	1.9999×10^{-5}
49	2.0955×10^{-4}	3.4559×10^{-6}

Table 4
Error between the exact and the FD-HMM solutions for time dependent oscillating coefficients and various number of coarse points (spatial discretization)

nb Coarse	Error (Euclidean)	Error (maximum)
9	1.9281×10^{-2}	3.2979×10^{-3}
19	2.4209×10^{-3}	4.1409×10^{-4}
29	7.7147×10^{-5}	1.3196×10^{-5}

Table 5
Error between the solution with small scale recovering and a reference solution

Small scale (coarse)	Error (Euclidean)	Error (maximum)
1999 (9)	3.6706×10^{-2}	9.6945×10^{-4}
1999 (19)	1.8949×10^{-2}	2.2396×10^{-4}

the spatial discretization of the microscopic solver. The error is computed on the fine grid (compared with a reference solution). We did the reconstruction starting with a coarse grid with $N = 9$ and $N = 19$ points.

3.3. Example 2: rough non-periodic (random) coefficient

We apply next the FD-HMM method at a problem with a rough (random) coefficient $a^\varepsilon(x)$ known to have an ε-correlation. This ε will be the ε-cell for the application of the finite difference method (see Section 2.2). This indicates how the method behaves for random correlated signal.

We briefly explain how we construct such an example. We first take an uniformly random distributed signal $s(x)$ in $[0.1, 1.1]$. We next discretize the interval $0 \leqslant x \leqslant 1$ in N equidistant point x_i. We define a "kernel" $g^\varepsilon(x)$ such that

$$g^\varepsilon(0) = 1/\varepsilon, \quad g^\varepsilon(x) = 0 \quad \text{if } x \notin (-\varepsilon/2, \varepsilon/2) \quad \text{and} \quad \int_{-\varepsilon/2}^{\varepsilon/2} g^\varepsilon(x)\,\mathrm{d}x = 1. \tag{61}$$

For each point of the discretization x_i we define

$$a^\varepsilon(x_i) = (g^\epsilon * s)(x_i) = \int_{-\varepsilon/2}^{\varepsilon/2} g^\varepsilon(x_i - z)s(z)\,\mathrm{d}z. \tag{62}$$

We chose

$$g^\varepsilon(x) = \frac{1}{\varepsilon}(1 - \sin 2\pi x/\varepsilon).$$

Finally, we take the same Eq. (56) as in the previous example and replace the oscillating coefficient by $a^\varepsilon(x)$ constructed above. The correlation was first chosen such that $\varepsilon = 10^{-2}$.

We plotted in Fig. 5 (left) the obtained signal. The relaxation time as shown in Fig. 4 is close to 3×10^{-5}.

In Fig. 5 (right) we plotted, the reference and the FD-HMM solutions for a mesh with $nb = 29$ coarse points and in Table 6 we compare the error for mesh refinement (with $nstep = 30{,}000$).

Remark 5. Notice that we consider the exact solution as a deterministic problem with rough coefficient generated "randomly" as explained above. We thus do not consider several realization, since the fine scale signal a^ε is fixed. We generate this rough fine scale signal a^ε on a fine grid with $\Delta x = 1/2000$ and we used the full resolution of the signal for the reference solution.

Dependence of the error on the size of the micro-cell. Unlike the case of periodic coefficients it is likely that for rough coefficients with correlation, increasing the size of the cell for the microscopic solver, will improve the result. In the following example, we took the same equation and coefficients as previously except the fact that we decrease the value of ε to $\varepsilon = 10^{-3}$. For a given number of coarse point, we increase the number of the cells for the microscopic solver between each coarse step.

We see in Tables 7 and 8 that choosing more ε-cell decreases the error. Notice that even with larger cells, FD-HMM is still more efficient for solving this problem than full scale resolution. For example choosing 5

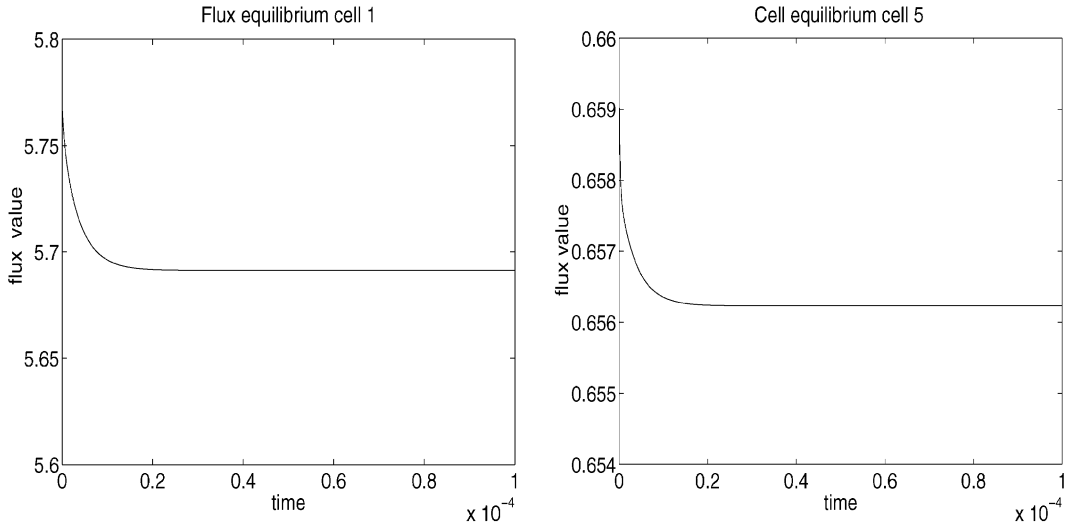

Fig. 4. The average flux $\bar{\boldsymbol{p}}^{\varepsilon}(t) = \sum_{i=1}^{s} a^{\varepsilon}(x_i)(\mathrm{d}/\mathrm{d}x)\bar{\boldsymbol{u}}^{\varepsilon}(t, x_i)$ for various ε-cells.

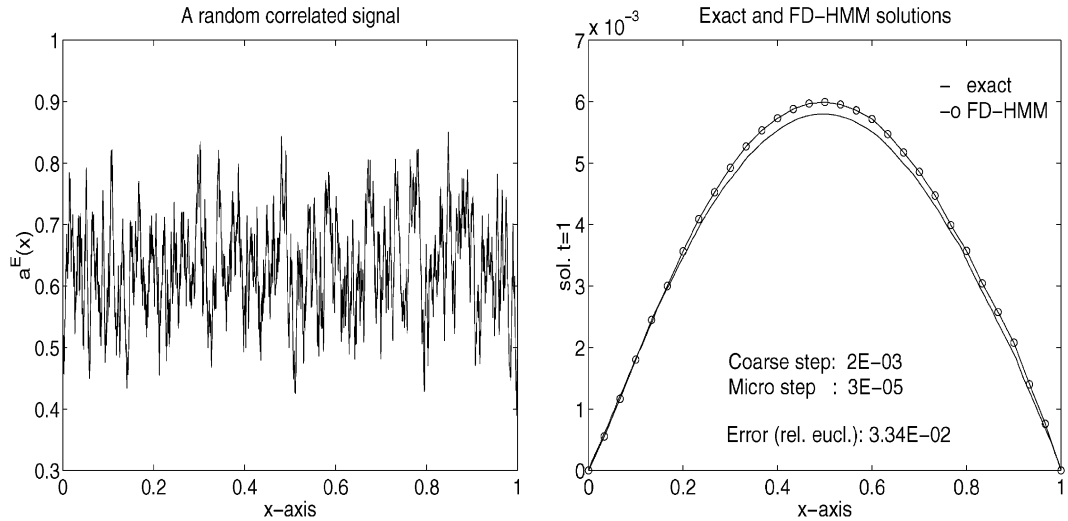

Fig. 5. Random correlated signal (left) and error between exact and FD-HMM solutions for 29 coarse points (right).

Table 6
Error between the exact and the FD-HMM solutions for increasing number of coarse points (spatial discretization)

Coarse step	Error (Euclidean)	Error (maximum)
9	1.0771×10^{-1}	5.7194×10^{-4}
19	1.3617×10^{-1}	7.5779×10^{-4}
29	4.0441×10^{-2}	2.0062×10^{-4}
39	3.6209×10^{-2}	1.8660×10^{-4}
49	1.2189×10^{-1}	6.6998×10^{-4}

Table 7
Error between the exact and the FD-HMM solutions for increasing number of cells, 9 coarse points

nb Cells	Error (Euclidean)	Error (maximum)	*nb* Cells	Error (Euclidean)	Error (maximum)
1	1.5661×10^{-1}	8.5611×10^{-4}	15	1.7133×10^{-2}	1.3260×10^{-4}
5	3.5796×10^{-2}	1.9935×10^{-4}	20	1.4452×10^{-2}	1.0827×10^{-4}
10	1.7592×10^{-2}	1.1278×10^{-4}			

Table 8
Error between the exact and the FD-HMM solutions for increasing number of cells, 19 coarse points

nb Cells	Error (Euclidean)	Error (maximum)	*nb* Cells	Error (Euclidean)	Error (maximum)
1	5.8031×10^{-1}	4.2010×10^{-4}	15	1.1218×10^{-2}	9.6756×10^{-5}
5	3.1749×10^{-2}	1.5329×10^{-4}	20	5.8617×10^{-3}	4.3328×10^{-5}
10	2.8356×10^{-2}	1.4710×10^{-4}			

ε-cell, for $nb = 9$ and for $\Delta\xi = \varepsilon/20$ (chosen as to have a good resolution of the small oscillation for the microscopic solver) we have to solve 1050 equations for the cell problems (the main cost of the FD-HMM), while the resolution by standard finite difference method, with $\varepsilon = 10^{-3}$, would need 19,999) equations for the same resolution as used for the microscopic solver.

To choose in an automatic way the number of cells which should be taken, we can at selected time step apply the FD-HMM method with different number of ε-cells. The difference of the solutions (which should tend to zero) gives an estimation of the appropriate (number of) ε-cell.

As in the previous periodic example, the FD-HMM can be applied to problems with rough non-periodic coefficients with time dependency.

3.4. Example 5: two dimensions

We consider the problem (1) in two dimensions with an oscillating coefficients given by

$$a^{\varepsilon}(x_1, x_2) = a \cdot \left(b + \sin \frac{2\pi(x_1 + x_2)}{\varepsilon} \right) \cdot I, \tag{63}$$

where I is the identity matrix. The coefficient a^{ε} has oscillations which are not in one of the two spatial directions.

We chose $a = 0.5$, $b = 1.1$ and $\varepsilon = 0.04$, Dirichlet boundary conditions and initial condition given by

$$u(0, x1, x_2) = 10x_1(1 - x_1^2)x_2(1 - x_2^2). \tag{64}$$

We plot in Fig. 6 (left) a reference solution (computed on a grid of 1999×1999 but displayed on a much coarser grid).

The coarse solution is evolved on a spatial grid of 9×9 interior points, thus $\Delta x = 1/10$. For the cell computation on 180 domains of measure ε^2 with $\varepsilon = 0.04$, we solve the original equations with a mesh of size $\Delta\xi = \varepsilon/20$. A similar resolution for the original equation with standard finite difference, leads to a mesh of 499×499 interior points.

The time evolution of the solution (from $t = 0$ to $t = 0.1$) is done in 1000 steps. We plot in Fig. 3 (right) the result at $t = 0.1$ for the FD-HMM.

Finally, we show in Fig. 7 how badly the solution is destroyed if we do not resolve the scale (we solve the original equation with 9×9 interior points).

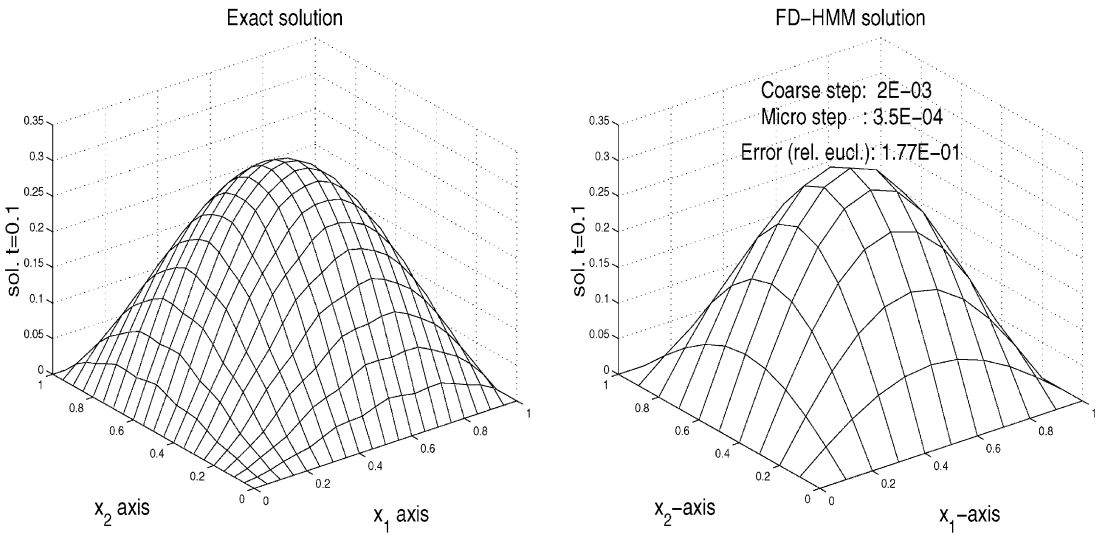

Fig. 6. 2D oscillating parabolic PDEs, reference (left) and FD-HMM solutions (right).

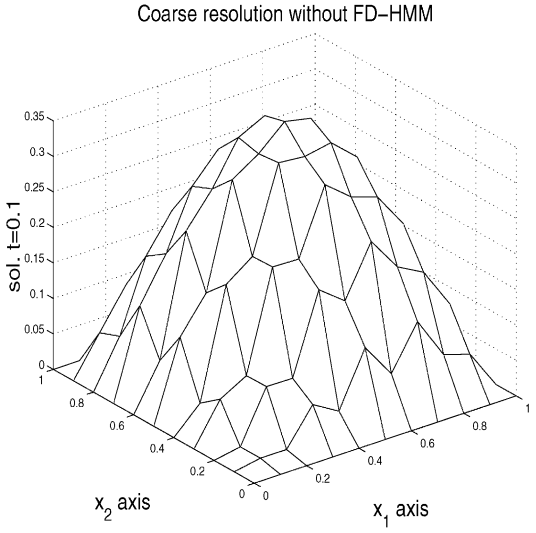

Fig. 7. 2D oscillating parabolic PDEs, resolution with 9×9 coarse points (spatial discretization) without using FD-HMM.

2d Rough non-periodic coefficients. We take the same problem as before, but with $a^\varepsilon(x,t)$ given by

$$(t+0.1)\begin{pmatrix} a_1(x) & 0 \\ 0 & a_2(x) \end{pmatrix},$$

where $a_1(x)$ and $a_2(x)$ are rough non-periodic (random) correlated coefficients constructed as in (62). The coefficients are different but have both the same correlation $\varepsilon = 10^{-2}$.

The coarse solution is evolved on a spatial grid of 9×9 interior points, as in the previous example. For the cell computation on 180 domains of length ε^2 with $\varepsilon = 0.01$ (the correlation length), we solve the ori-

ginal equations with a mesh of size $\Delta\xi = \varepsilon/20$. A similar resolution for the original equation with standard finite difference, leads to a mesh of 1999×1999 interior points. The time evolution of the solution (from $t = 0$ to $t = 0.1$) is done in 1000 steps. We obtain for the error $\mathrm{err}_2 = 5.56 \times 10^{-1}$ and $\mathrm{err}_\infty = 3.06 \times 10^{-1}$ for the weighted Euclidean and maximum norm, respectively.

Acknowledgements

The work of Abdulle is partially supported by the Swiss National Science Foundation and an ONR Grant N00014-01-1-0674 during his stay in Princeton. The work of E is supported in part by an ONR Grant N00014-01-1-0674.

References

[1] A. Abdulle, Fourth order Chebyshev methods with recurrence relation, SIAM J. Sci. Comput. 23 (6) (2002) 2041–2054.
[2] A. Abdulle, A.A. Medovikov, Second order Chebyshev methods based on orthogonal polynomials, Numer. Math. 90 (1) (2001) 1–18.
[3] G. Allaire, Homogenization and two-scale convergence, SIAM J. Math. Anal. 23 (6) (1992) 1482–1518.
[4] I. Babuska, Homogenization and its applications, in: B. Hubbard (Ed.), SYNSPADE, 1975, pp. 89–116.
[5] A. Bensoussan, J.-L. Lions, G. Papanicolaou, Asymptotic Analysis for Periodic Structures, North-Holland, Amsterdam, 1978.
[6] D. Cioranescu, P. Donato, An Introduction to Homogenization, Oxford University Press, Oxford, 1999.
[7] W. E, Homogenization of linear and nonlinear transport equations, Commun. Pure Appl. XLV (1992) 301–326.
[8] W. E, B. Engquist, The heterogeneous multi-scale methods, Comm. Math. Sci. 1 (1) (2003) 87–132.
[9] B. Engquist, Computation of oscillatory solutions to hyperbolic differential equations, Springer Lecture Notes Math. 1270 (1987) 10–22.
[10] M. Dorobantu, B. Engquist, Wavelets-based numerical homogenization, SIAM J. Numer. Anal. 35 (2) (1998) 540–559.
[11] B. Engquist, O. Runborg, Wavelets-based numerical homogenization with applications, in: Multiscale and Multiresolution Methods, Lecture Notes in Computational Science and Engineering, vol. 20, Springer, Berlin, 2002, pp. 97–148.
[12] E. Hairer, S.P. Nørsett, G. Wanner, Solving ordinary differential equations I. Nonstiff problems, Springer Series in Computational Mathematics, vol. 8, second ed., Springer, Berlin, 1993.
[13] E. Hairer, G. Wanner, Solving ordinary differential equations II. Stiff and differential-algebraic problems, Springer Series in Computational Mathematics, vol. 14, second ed., Springer, Berlin, 1996.
[14] T.-Y. Hou, X.-H. Wu, A multiscale finite element method for elliptic problems in composite materials and porous media, J. Comput. Phys. 134 (1997) 169–189.
[15] T.-Y. Hou, X.-H. Wu, Z. Cai, Convergence of a multi-scale finite element method for elliptic problems with rapidly oscillating coefficients, Math. Comput. 68 (227) (1999) 913–943.
[16] J.L. Lions, E. Magenes, Problèmes aux limites non homogènes et applications, vols. 1 and 2, Paris, Dunod, 1968 (English Transl., Springer, 1970).
[17] G. Nguetseng, A general convergence result for a functional related to the theory of homogenization, SIAM J. Math. Anal. 20 (3) (1989) 608–623.
[18] A-M. Matache, I. Babuska, C. Schwab, Generalized p-FEM in homogenization, Numer. Math. 86 (2) (2000) 319–375.
[19] C. Schwab, A.-M. Matache, Generalized FEM for homogenization problems, in: Multiscale and Multiresolution Methods, Lecture Notes in Computational Science and Engineering, vol. 20, Springer, Berlin, 2002, pp. 197–238.
[20] N. Neuss, W. Jäger, G. Wittum, Homogenization and multigrid, Computing 66 (1) (2001) 1–26.